Available online at www.sciencedirect.com
SCIENCE DIRECT®
International Journal of Thermal Sciences 43 (2004) 865–876
International Journal of Thermal Sciences
www.elsevier.com/locate/ijts

Numerical study of natural convection with surface radiation in side-vented open cavities

S.N. Singh, S.P. Venkateshan *

Heat Transfer and Thermal Power Laboratory, Department of Mechanical Engineering, Indian Institute of Technology Madras, Chennai 600 036, India

Received 9 June 2003; received in revised form 17 December 2003; accepted 12 January 2004

Available online 9 April 2004

Abstract

The paper presents a numerical study of steady combined laminar natural convection and surface radiation heat transfer in a two-dimensional side-vented open cavity for different aspect ratios, side-vent ratios, and surface emissivities using air as the fluid medium. Results have been compared with experimental results available in the literature. Surface radiation is found to alter the basic flow pattern as well as the thermal performance substantially. The numerical investigation provides evidence of the existence of thermal boundary layers along adiabatic walls of the cavity as a consequence of the interaction of natural convection and surface radiation. Based on numerical data correlations have been developed for convective as well as radiative heat transfer.

Keywords: Natural convection; Surface radiation; Side-vent; Stream function; Vorticity

1. Introduction

Despite significantly lower values of the convective heat transfer coefficient, cooling by natural convection using air is preferred, for example, in numerous electronic cooling applications because of its low cost, inherent reliability, simplicity and noiseless method of thermal control. In natural convection systems, even moderate temperature differences give rise to significant radiation effects so that the radiative and convective contributions may become comparable and thus influence the total heat transfer rate. It is therefore unrealistic to ignore interaction of surface radiation and convection. In an open cavity there is a continuous intake of fresh air from the ambient and exhaust of heated air back to the ambient and hence stratification effects are reduced. Thus, it offers one method of heat dissipation from electronic equipment and, to protect the components from external disturbances, housing the components in a slot may be required, although mounting it on a vertical flat plate may be advantageous for both convective and radiative heat transfer. How the opening affects the flow and temperature fields is an important outcome of the present study. The present study simulates the cooling of an electronic component placed in a slot similar to the one considered experimentally by Ramesh and Merzkirch [1]. Natural convection in cavities with openings has received a sustained attention in the heat transfer literature [2–16]. Those that are important among them either directly or indirectly, from the present point of view, are discussed here. Abib and Jaluria [6] numerically investigated a partially open enclosure having all sides insulated with a heat source at the bottom of the left wall and a partially open right wall. They used open boundary condition at partial opening. Angirisa and Mahajan [10] numerically analyzed free convection from L-shaped corners with adiabatic and cold isothermal walls. They discussed the importance of using proper boundary conditions along the open boundaries. Rodighiero and de Socio [4] experimentally analyzed L-shaped corners with adiabatic bottom wall. Balaji and Venkateshan [14] studied the same problem using finite volume based method that used the vorticity-stream function formulation of the governing equations. Ramesh et al. [15] provided results of experiments using Differential Interferometer and also semi-experimental results for an open cavity having left heated wall and bottom and right adiabatic walls for a range of Rayleigh number, aspect ratio, and emissivity. Both these studies included the effect of surface radiation.

* Corresponding author.
E-mail addresses: snsingh63@yahoo.com (S.N. Singh), spv@iitm.ac.in (S.P. Venkateshan).

1290-0729/$ – see front matter
doi:10.1016/j.ijthermalsci.2004.01.002

Nomenclature

A	aspect ratio, $= H/d$
d	spacing ..... m
F_{ij}	view factor between element i and element j
g	acceleration due to gravity ..... $\mathrm{m\cdot s^{-2}}$
G'	elemental irradiation ..... $\mathrm{W\cdot m^{-2}}$
G	elemental dimensionless irradiation, $= G'/\sigma T_h^4$
Gr_H	Grashof number based on H, $= g\beta(T_h - T_\infty)H^3/\nu^2$
H	height of the cavity ..... m
h_T	height of the total computational domain .... m
J'	elemental radiosity ..... $\mathrm{W\cdot m^{-2}}$
J	elemental dimensionless radiosity, $= J'/\sigma T_h^4$
k	thermal conductivity of fluid ..... $\mathrm{W\cdot m^{-1}\cdot K^{-1}}$
m	number of grid points in horizontal direction in the computational, domain
n	number of grid points in vertical direction in the computational domain
N_{rc}	radiation conduction parameter, $= \sigma T_h^4 d/[(T_h - T_\infty)k]$
Nu_c	convection Nusselt number, $= -(\frac{\partial\theta}{\partial Y})$ at $Y = 0$, or $Y = 1$ as needed
$\overline{Nu}_c$	average convection Nusselt number, $= -\frac{1}{A}\int_0^A Nu_c \,\mathrm{d}Y$
Nu_R	radiation Nusselt number, $= N_{\mathrm{rc}}(J - G)$
$\overline{Nu}_R$	average radiation Nusselt number, $= \frac{1}{A}\int_0^A Nu_R \,\mathrm{d}Y$
$\overline{Nu}_t$	average total convection and radiation Nusselt number, $= \overline{Nu}_c + \overline{Nu}_R$
Pr	Prandtl number, $= \nu/\alpha$
Q_c	heat transfer due to convection ..... W
Q_R	heat transfer due to radiation ..... W
Ra_H	Rayleigh number based on H, $= Gr_H Pr$
T	temperature ..... K
T_h	temperature of left wall of the cavity ..... K
T_∞	ambient temperature ..... K
T_R	temperature ratio, $= T_\infty/T_h$
u	vertical velocity ..... $\mathrm{m\cdot s^{-1}}$
U	dimensionless vertical velocity, $= ud/\alpha$
v	cross velocity ..... $\mathrm{m\cdot s^{-1}}$
V	dimensionless cross velocity, $= vd/\alpha$
w	vent height ..... m
W	vent ratio, $= w/H$
W_1	port ratio, $= w_1/H$
x	vertical coordinate ..... m
X	dimensionless vertical coordinate, $= x/d$
y	horizontal coordinate ..... m
Y	dimensionless horizontal coordinate, $= y/d$

Greek symbols

α	fluid thermal diffusivity ..... $\mathrm{m^2\cdot s^{-1}}$
β	isobaric coefficient of volumetric thermal expansion ..... $\mathrm{K^{-1}}$
ε	emissivity of the walls
ν	kinematic viscosity of the fluid ..... $\mathrm{m^2\cdot s^{-1}}$
θ	dimensionless temperature, $= (T - T_\infty)/(T_h - T_\infty)$
ψ'	stream function ..... $\mathrm{m^2\cdot s^{-1}}$
ψ	dimensionless stream function, $= \psi'/\alpha$
σ	Stefan Boltzmann constant, $= 5.67 \times 10^{-8}\ \mathrm{W\cdot m^{-2}\cdot K^{-4}}$
ω'	vorticity ..... $\mathrm{s^{-1}}$
ω	non-dimensional vorticity, $= \omega' d^2/\nu$
δ	convergence parameter in percentage, $= \lvert(\zeta_{\mathrm{new}} - \zeta_{\mathrm{old}})/\zeta_{\mathrm{new}}\rvert \times 100$
ζ	dependent variable $(\psi, \omega, \theta, J, G)$ over which convergence test is applied

Subscripts

c	convection
H	based on height of the left wall of the side-vented cavity
h	hot
i, j	any two arbitrary area elements of an enclosure used in radiation analysis
new, old	values of the dependent variables $(\psi, \omega, \theta, J, G)$ obtained from the present and previous iterations, respectively
R	radiation
rc	radiation conduction
T	total height
t	total average
∞	ambient
l	right open portion

Superscript

$'$	dimensional value

Apart from applications mentioned earlier, the present study is important from a fundamental point of view. The proper choice of the boundary condition across the open boundaries is essential to properly understand the flow physics. The proper choice of the boundary conditions across opening helps in restricting the computational domain and hence helps in saving of computational effort. The present study also presents numerically the effects of surface radiation on natural convection in side-vented open cavities for a wide range of parameters and develops correlations for convective and radiative Nusselt numbers based on a detailed numerical study.

2. Mathematical formulation

2.1. Formulation for convection

The two-dimensional, steady, incompressible, laminar natural convection heat transfer from a side-vented cavity

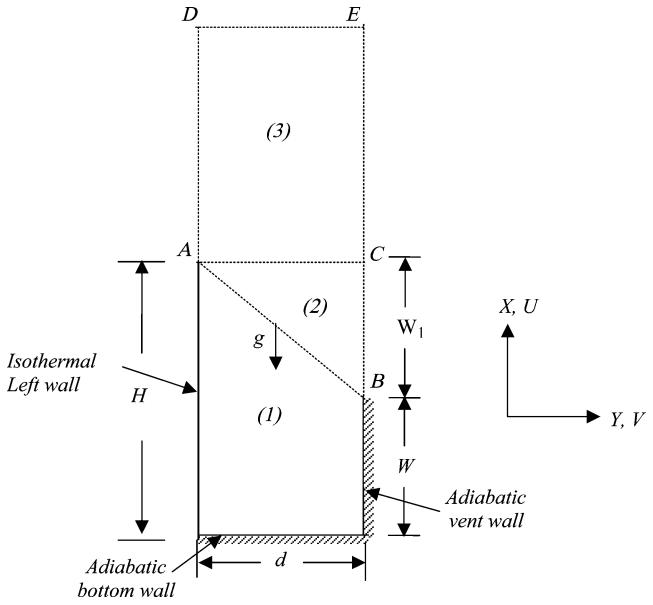

Fig. 1. Schematic of the problem geometry showing the computational domains.

with a height H, spacing d and vent wall height w, is considered using the system of coordinates shown in Fig. 1. The governing equations in stream function (Ψ) vorticity (ω) form, for a constant property fluid under the Boussinesq approximation, in the non-dimensional form are:

$$U\frac{\partial\omega}{\partial X}+V\frac{\partial\omega}{\partial Y}=Pr\left[\frac{\partial^2\omega}{\partial X^2}+\frac{\partial\omega^2}{\partial Y^2}\right]-Ra\frac{\partial\theta}{\partial Y} \tag{1}$$

$$\frac{\partial^2\psi}{\partial X^2}+\frac{\partial^2\psi}{\partial Y^2}=-Pr\,\omega \tag{2}$$

$$U\frac{\partial\theta}{\partial X}+V\frac{\partial\theta}{\partial Y}=\frac{\partial^2\theta}{\partial X^2}+\frac{\partial^2\theta}{\partial Y^2} \tag{3}$$

where $U=\frac{\partial\psi}{\partial Y}$, $V=-\frac{\partial\psi}{\partial X}$ and $\omega=\frac{\partial V}{\partial X}-\frac{\partial U}{\partial Y}$

2.2. Formulation for radiation

The radiosity-irradiation formulation is used to describe surface radiation (Balaji and Venkateshan [11]). For an area element on a boundary of the cavity the non-dimensional radiosity is given by the equation

$$J_i=\varepsilon(T_i/T_h)^4+(1-\varepsilon)\sum_{j=1}^{2(m+n-2)}F_{ij}J_j$$

$$i=1,2(m+n-2) \tag{4}$$

The walls are assumed diffuse and gray. At the adiabatic bottom and right walls convection and radiation balance each other. Hence

Bottom wall:

$$-\frac{\partial\theta}{\partial X}=N_{\mathrm{rc}}(J-G) \tag{5}$$

Right wall:

$$\frac{\partial\theta}{\partial Y}=N_{\mathrm{rc}}(J-G) \tag{6}$$

The view factors F_{ij} are evaluated using Hottel's crossed-string method [18].

2.3. Computational domain

From a purely practical point of view one would like to know the flow and temperature fields in the domain labeled (1) in Fig. 1. However, this choice for the computational domain would need the specification of the boundary conditions along the inclined line AB joining the topmost point of the left wall and the topmost point of the right wall. In view of the difficulty in specifying the proper boundary condition along AB it is convenient to extend the domain by including the triangular domain (2) also in the computational domain. A third possibility that seems to be appropriate is to include an extension (3) in the computational domain. However, extension of the domain in the last three cases requires the specification of the boundary conditions along the boundaries of the respective extended domains. The selection of domain and the appropriate boundary conditions is based on a numerical experiment presented later. Another possibility that one may think of is to extend the computational domain to include a region to the right of the opening on the right wall. The last one is not considered in the present study. The primary reason for this is the lack of information regarding the nature of the right adiabatic wall, its thickness and thermal properties used in [1]. Further assumptions and simplifications would have to be made that may in fact be hard to validate.

In fact, in their study of natural convection in a side open cavity, Polat and Bilgen [16] did restrict the computational domain by specifying suitable boundary conditions across the side opening. The boundary conditions were justified based on the flow and temperature fields within the cavity region in comparison with those that were obtained with extended computational domain. Radiation was not considered in that study. That there is no uniqueness about the boundary conditions to be used across openings is clear from the various boundary conditions that have been used in earlier studies. In the present problem there are multiple openings and surface radiation plays an important interactive role along with natural convection. Hence the appropriate boundary conditions are to be found by studying the streamline patterns and temperature distribution within the cavity. Though there may be many possibilities those that hold promise in the present type of situation only have been dealt with.

2.4. Boundary conditions

The boundary conditions are specified for stream function and vorticity on all the boundaries based on Balaji and Venkateshan [11] and Gururaja Rao et al. [17]. The boundary conditions on U and V are also indicated for the sake of clarity. Left isothermal wall:

$$Y=0,\qquad 0<X<A,\qquad U=0,\qquad V=0\quad\text{or}$$

$$\psi = 0, \qquad \theta = 1, \qquad \omega = -\frac{1}{Pr}\frac{\partial^2 \psi}{\partial Y^2} \tag{7}$$

Bottom wall:

$$X = 0, \qquad 0 < Y < 1, \qquad U = 0, \qquad V = 0 \quad \text{or}$$
$$\psi = 0, \qquad \omega = -\frac{1}{Pr}\frac{\partial^2 \psi}{\partial X^2}, \qquad -\frac{\partial \theta}{\partial X} = N_{\mathrm{rc}}(J - G) \tag{8}$$

Side-vent wall:

$$Y = 1, \qquad 0 < X < W, \qquad U = 0, \qquad V = 0 \quad \text{or}$$
$$\psi = 0, \qquad \omega = -\frac{1}{Pr}\frac{\partial^2 \psi}{\partial Y^2}, \qquad \frac{\partial \theta}{\partial Y} = N_{\mathrm{rc}}(J - G) \tag{9}$$

Extended domain (1) + (2):

Along the boundary BC there are several options. They are:

$$\text{(I)} \qquad Y = 1, \qquad W < X < A, \qquad U = \frac{\partial \psi}{\partial Y} = 0$$
$$\frac{\partial V}{\partial Y} = \frac{\partial^2 \psi}{\partial X \partial Y} = 0 \tag{10}$$

The vertical velocity U is set to zero. The boundary condition on V, the cross velocity, is obtained from continuity equation as $\frac{\partial V}{\partial Y} = 0$. These velocity boundary conditions were partially implemented by Abib and Jaluria [6] in partially open enclosures. They set vertical velocity ($U = 0$) on right open part but did not implement the condition $\frac{\partial V}{\partial Y} = 0$ because the fluid enters and leaves from the same opening. Angirasa and Mahajan [10] used the same velocity boundary condition as that used in Abib and Jaluria [6] on right open boundary in a partially open cavity.

$$\text{(II)} \qquad Y = 1, \qquad W < X < A, \qquad V = -\frac{\partial \psi}{\partial X} = 0$$
$$\frac{\partial U}{\partial X} = \frac{\partial^2 \psi}{\partial X \partial Y} = 0 \tag{11}$$

The cross velocity V is set at zero, then the boundary condition on the vertical velocity, is obtained from equation of continuity as $\frac{\partial U}{\partial X} = 0$.

$$\text{(III)} \qquad Y = 1, \qquad W < X < A, \qquad \omega = 0$$
$$A < X < 2A, \qquad \frac{\partial U}{\partial X} = \frac{\partial V}{\partial Y} = \frac{\partial^2 \psi}{\partial X \partial Y} = 0 \tag{12}$$

Neither U nor V is assumed to be zero in this case. The mixed boundary condition provides "smooth" variation of velocity components across the opening. By definition of stream function the equation of continuity is satisfied everywhere. However, the smoothness conditions make the equation of continuity satisfied all along the boundary identically by making both the derivatives zero along the opening. Gururaja Rao et al. [17] have implemented the above boundary condition on the right side of computational domain of a heated vertical plate in mixed flow, in the presence of surface radiation. After studying the flow pattern they concluded that this boundary condition is the most appropriate.

Along the boundary AC:

The boundary conditions proposed by Balaji and Venkateshan [11] are made use of as given below:

$$X = A, \qquad 0 < Y < 1, \qquad \frac{\partial \psi}{\partial X} = 0, \qquad \frac{\partial \omega}{\partial X} = 0$$
$$U = \frac{\partial \psi}{\partial Y} > 0, \qquad \frac{\partial \theta}{\partial X} = 0, \quad \text{or} \quad U = \frac{\partial \psi}{\partial Y} < 0$$
$$V = -\frac{\partial \psi}{\partial X} = 0, \qquad \theta = 0 \tag{13}$$

Extended domain (1) + (2) + (3):

Along the left boundary AD of the extended domain, we have, by symmetry

$$Y = 0, \qquad A < X < 2A, \qquad V = -\frac{\partial \psi}{\partial X} = 0$$
$$\frac{\partial \theta}{\partial Y} = 0 \tag{14}$$

Along the right side extended boundary BE:

Three options as in the case of boundary BC.

Along the boundary DE:

$$X = A, \qquad 0 < Y < 1, \qquad \omega = 0, \qquad U = \frac{\partial \psi}{\partial Y} > 0$$
$$\frac{\partial \theta}{\partial X} = 0, \quad \text{or} \quad U = \frac{\partial \psi}{\partial Y} < 0, \qquad V = -\frac{\partial \psi}{\partial X} = 0$$
$$\theta = 0 \tag{15}$$

3. Method of solution

The governing equations (1)–(3) are first transformed into finite difference equations using a finite-volume based finite difference method of Gosman et al. [19]. Gauss–Seidel iterative procedure is used to solve the resulting algebraic equations. A 31×51 non-uniform grid system for the computational domain is employed. The grid sizes have been fixed based on grid sensitivity analysis, the results of which are presented in the ensuing section. A semi-cosine function and a cosine function have been chosen to generate the grids respectively along the X and Y directions in the cavity region. Uniform grids are used in region (3) along the X direction. The use of semi-cosine function ensures very fine grids near the boundaries, where the gradients are steep, with progressively coarser grids in the rest of the domain. The grid patterns used are shown in Fig. 2(a) and (b). With reference to the implementation of derivative boundary conditions, three point formulae using second degree Lagrangian polynomial have been used. Upwinding has been used for representing the advection terms. This ensures stable and convergent solutions. The integrations required in all the calculations are performed using Simpson's 1/3 rule for non-uniform step size. Under relaxation with a relaxation parameter of 0.5 was used for all three equations and the radiosity equations

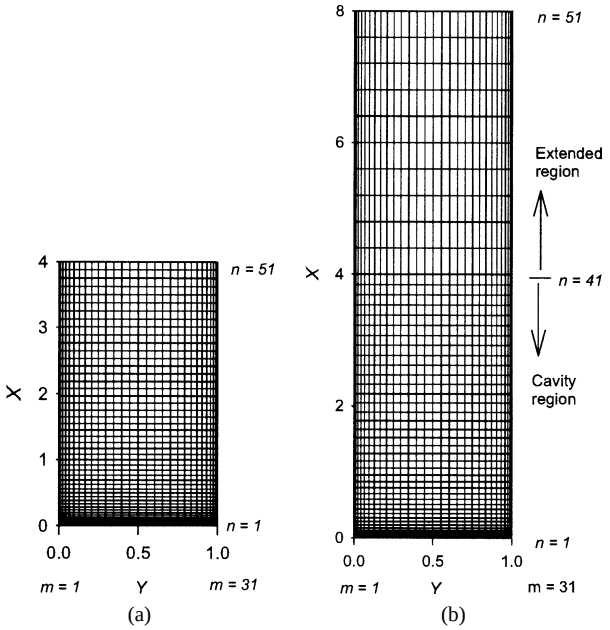

Fig. 2. Typical grid patterns used in the analysis: (a) Grid size $= 31 \times 51$, $A = 4$, $H_T = H$, $W = 0.5$; (b) Grid size $= 31 \times 51$, $A = 4$, $H_T = 2H$, $W = 0.5$.

to obtain convergent results. A convergence criterion (δ), in percentage form, has been defined as

$$\delta = \left|(\zeta_{\text{new}} - \zeta_{\text{old}})/\zeta_{\text{new}}\right| \times 100 \tag{16}$$

where ζ is any dependent variable $(\psi, \omega, \theta, J, G)$ over which the convergence test is applied, while the subscripts "old" and "new" represent the values of ζ calculated from two successive iterations. A convergence criterion of 0.1% has been used on stream function and temperature, while on vorticity, a convergence criterion of 0.5% has been used. A convergence criterion of 0.01% has been used for the radiosity.

4. Results and discussion

Table 1 shows the range of parameters considered in the present study. Calculations have been made keeping in view the objective of evolving useful correlations for the radiation and convection Nusselt numbers. Before proceeding further the result of a grid sensitivity study is presented.

4.1. Grid sensitivity study

Tables 2(a) and 2(b) show the effect of the grid size on the solution for a typical case with $Ra_H = 1.075 \times 10^6$, $A = 4$, $W = 0.5$, $N_{\text{rc}} = 70.774$, $T_R = 0.844$, $\varepsilon_L = \varepsilon_b = \varepsilon_r = 0.85$. The present problem involves an interaction between natural convection and radiation. Since the grid size affects these two to different extents, it is necessary to look at the effect of grid size on both the convection and radiation Nusselt numbers in order to decide on the grid system that is to be used to get acceptable results. The computational domain

Table 1
Range of parameters considered in the present study

Parameters	Range
Rayleigh number, Ra_H	1.038×10^4–1.058×10^7
Conduction–radiation parameter, N_{rc}	3.924–46.175
Emissivity, ε	0.05–0.85
Temperature ratio, T_R	0.844–0.952
Aspect ratio, A	2–8
Vent ratio, W	0.25–0.50

Table 2(b)
Grid independence study $n = 31$, m varied ($Pr = 0.7$, $Ra_H = 1.075 \times 10^6$, $A = 4$, $W = 0.5$, $N_{\text{rc}} = 10.774$, $\varepsilon = 0.85$)

$m \times n$	$\overline{Nu}_c$	$\overline{Nu}_R$	$\overline{Nu}_t$	% change in $\overline{Nu}_c$ (abs)	% change in $\overline{Nu}_R$ (abs)	% change in $\overline{Nu}_t$ (abs)
21×31	12.711	13.641	26.352	–	–	–
31×31	12.097	13.663	25.760	4.830	0.161	2.246
41×31	11.859	14.154	26.013	1.967	3.593	0.982
51×31	11.726	14.859	26.585	1. 121	4.980	2.199
61×31	11.668	15.431	27.099	0.495	3.849	1.933

Table 2(b)
Grid independence study $m = 31$, n varied

$m \times n$	$\overline{Nu}_c$	$\overline{Nu}_R$	$\overline{Nu}_t$	% change in $\overline{Nu}_c$ (abs)	% change in $\overline{Nu}_R$ (abs)	% change in $\overline{Nu}_t$ (abs)
31×21	12.168	14.507	26.675	–	–	–
31×31	12.097	13.663	25. 760	0.583	5.818	3.430
31×41	12.030	13.649	25.679	0.554	0.102	0.314
31×51	12.017	13.780	25.797	0.108	0.960	0.459
31×61	11.980	13.747	25.727	0.308	0.239	0.271

considered is (1) + (2). The grid sensitivity analysis is done in two parts—(a) 'n' fixed with varying 'm' and (b) 'm' fixed—with varying 'n' and the optimum grid size is arrived at. It can be seen from Table 2(a) that the differences in $\overline{Nu}_c$ between the grid sizes of 51×31 and 61×31 is 0.495% which is the lowest. However, the differences in $\overline{Nu}_R$ and $\overline{Nu}_t$ are comparatively higher than for other grid sizes. The difference in $\overline{Nu}_R$ between the grid sizes of 21×31 and 31×31 is 0.161% is the lowest. However, the differences in $\overline{Nu}_c$ and $\overline{Nu}_t$ are the biggest. Also 21×31 is a relatively coarse grid. The difference in $\overline{Nu}_t$ between the grid sizes of 31×31 and 41×31 is the lowest and its $\overline{Nu}_c$ and $\overline{Nu}_R$ comparatively smaller than others. Based on these observations m has been fixed as 31. Similarly, Table 2(b) shows that the difference in $\overline{Nu}_t$ between the grid sizes of 31×51 and 31×61 is 0.271% which is the lowest and $\overline{Nu}_c$ and $\overline{Nu}_R$ have a comparatively smaller value than others. Based on these observations the n is chosen as 51. Thus the grid pattern used in the present study is 31×51.

An alternate way of looking at the data presented in Tables 2(a) and 2(b) is to consider the mean and deviation of the various values that have been calculated. In order to do this it was decided that the coarse grid corresponding to $m = n = 21$ be not considered since the changes in Nusselt number values are the largest when we change these

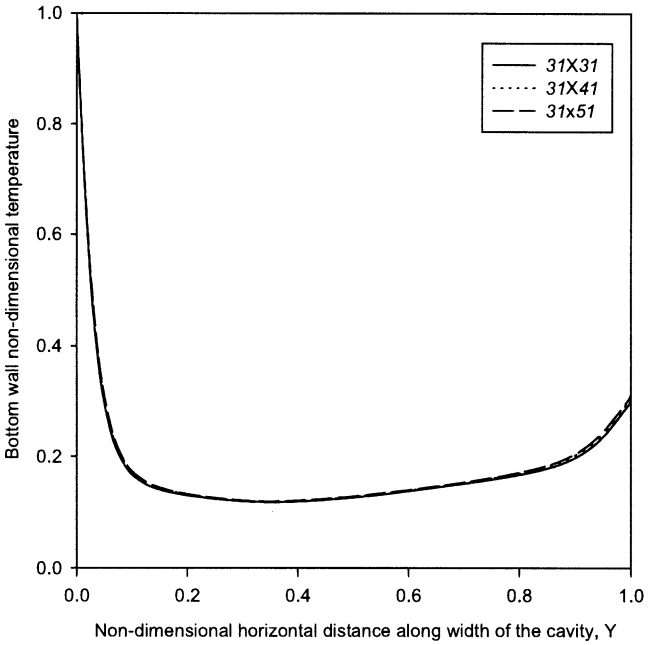

Fig. 3. Effect of grid size on the temperature variation at $X = 0$ for $Ra_H = 1.075 \times 10^6$, $A = 4$, $W = 0.5$, $\varepsilon = 0.85$, $T_R = 0.844$, $N_{\rm rc} = 10.774$.

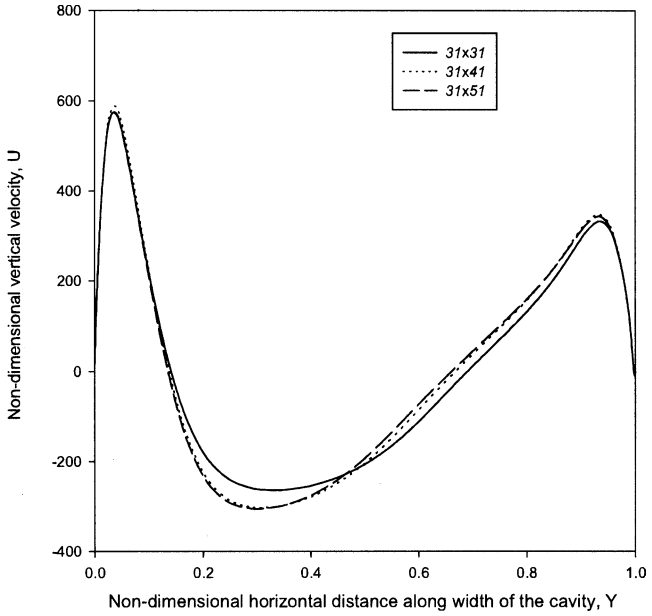

Fig. 4. Effect of grid size on the vertical velocity (U) $X = 1$ for $Ra_H = 1.075 \times 10^6$, $A = 4$, $W = 0.5$, $\varepsilon = 0.85$, $T_R = 0.844$, $N_{\rm rc} = 10.774$.

to 31. The mean convection Nusselt number is 11.93 with a deviation of ± 0.16 and mean total Nusselt number is 26.1 with a deviation of ± 0.48. The point that is being made is that the values converge within a reasonably small zone of confusion for the $m \times n$ range considered in the present numerical experiment.

It is noted that the total number of nodes in the domain has been varied from 651 to 1891, a three-fold increase from the lowest to the highest value. Further, when non-uniform grids are used, the smallest element reduces non-linearly with an increase in the number of nodes. Since the present study is confined to *laminar* natural convection only, it is not necessary to use very small grid sizes that are normally needed in turbulent flow calculations. Also the near wall features of flow and temperature fields are adequately resolved with 31×51 grids. This may be seen from Figs. 3 and 4 that show θ and U variations along the width of the cavity (i.e., with respect to Y) for three different grid sizes viz. 31×31, 31×41 and 31×51. There is hardly any effect of grid size on the temperature profile. The velocity profile, however, is affected marginally. The difference between the profiles obtained with 31×41 and 31×51 show very negligible change for all Y. It therefore is appropriate to choose 31×51 for further computations. We mention in passing that Balaji and Venkateshan [11] made use of 31×31 nodes in their treatment of similar problems.

4.2. Effects of different boundary conditions on flow patterns

Earlier we have mentioned the different types of boundary conditions that have been used in earlier studies in the relevant literature. The flow pattern will certainly be affected by the choice of the boundary condition. Consider the computational domain to be (1) + (2). The boundary condition (I) implies that the flow velocity is normal to the open boundary BC and the vertical velocity remains zero across BC. Fig. 5(a) shows the streamline and isotherm patterns for aspect ratios of 4 and surface emissivity of 0.80, corresponding to the case of strong radiation. The other parameters used are: $Ra_H = 1.075 \times 10^6$, $W = 0.5$, $T_R = 0.844$ and $N_{\rm rc} = 10.774$. It is seen that there is inflow across substantial part of the boundary BC and this flow reaches all the way to the bottom of the hot wall and then raises parallel to it. There is also some inflow across AC. There is a recirculating flow occupying a large part of the open cavity as shown. Thus there is considerable stratification in the right bottom part of the cavity.

The state of affairs is as shown in Fig. 5(b) when the boundary condition (II) is chosen along BC. There is complete blockage of flow across the opening BC. All the flow enters across AC. The recirculation pattern near the right bottom corner is not much different. The conditions prevailing when the boundary condition (III) is chosen across BC is shown in Fig. 5(c). There is inflow and outflow across both AC and BC. Because of radiant heating of the right wall a boundary layer type flow is expected next to it (Ramesh et al. [15] and Balaji and Venkateshan [11]). The interaction between the weaker plume next to the right wall and the inflow across the boundary BC gives rise to a complex feature near the top of the right wall. (It was verified that this feature is totally absent when radiation effect is ignored, by setting $\varepsilon = 0$. The boundary layer next to the right wall is absent.) The stratification near the right bottom part of the cavity is weaker compared to the previous two cases. The thermal boundary layer next to the hot wall shows

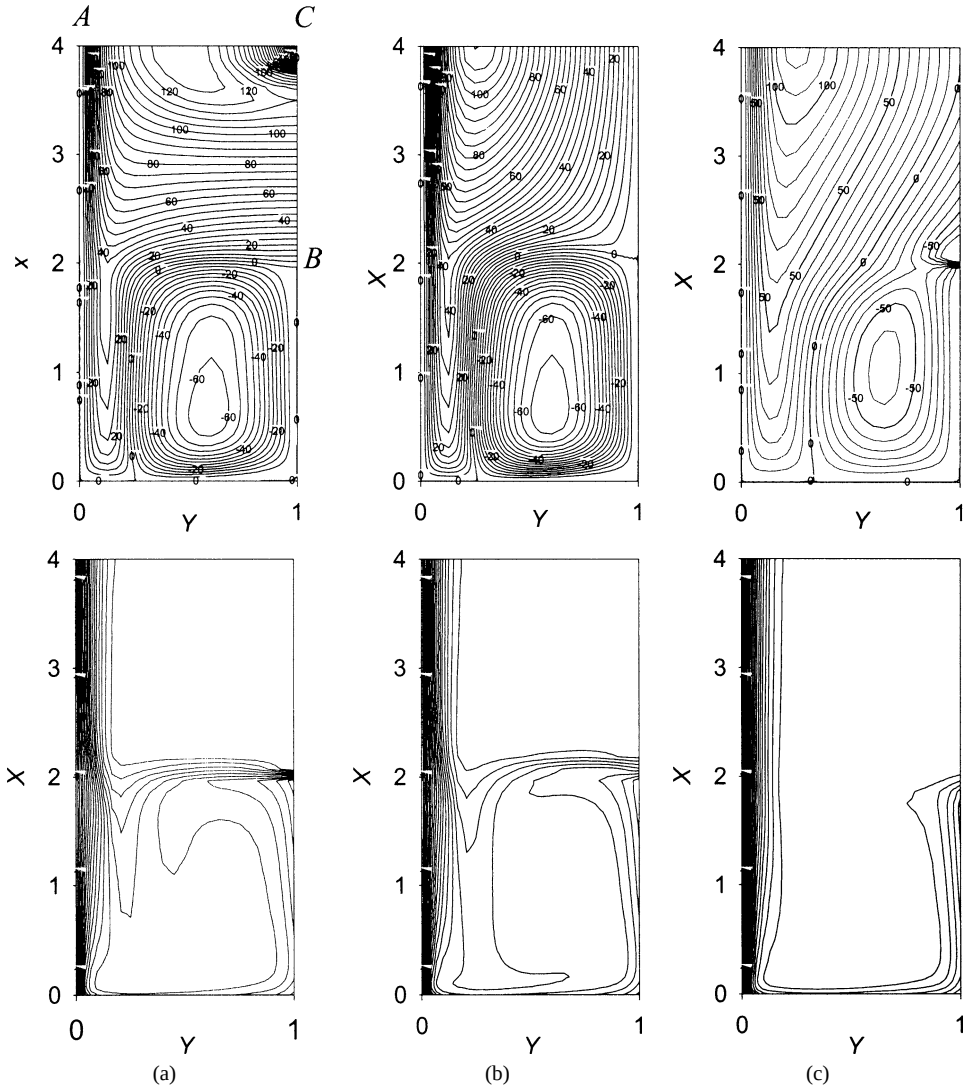

Fig. 5. Streamline and isotherm plots for combined natural convection and surface radiation with different velocity boundary conditions on the right open portion of the cavity for $Ra_H = 1.075 \times 10^6$, $A = 4$, $W = 0.5$, $\varepsilon = 0.80$, $T_R = 0.844$, $N_{\rm rc} = 10.774$: (a) $U = 0$; (b) $V = 0$; (c) $\frac{\partial U}{\partial X} = \frac{\partial V}{\partial Y} = 0$.

Table 3
Effect of Boundary condition along BC ($Pr = 0.7$, $Ra_H = 1.075 \times 10^6$, $A = 4$, $W = 0.5$, $\varepsilon = 0.05$, 0.80)

Boundary condition	$\overline{Nu}_c$		$\overline{Nu}_t$	
along BC	$\varepsilon = 0.05$	$\varepsilon = 0.80$	$\varepsilon = 0.05$	$\varepsilon = 0.80$
$V = 0$	12.333	10.180	13.301	21.331
$U = 0$	12.129	9.580	13.097	21.045
$\frac{\partial U}{\partial X} = \frac{\partial V}{\partial Y} = 0$	12.379	12.014	13.347	24.794

significant changes with the type of boundary condition used across BC. A study of Fig. 5(a)–(c) shows that the proper flow and temperature variations are obtained only with boundary condition (III) applied along BC.

With respect to heat transfer from the hot left wall of the cavity, Table 3 shows the results for two cases with weak ($\varepsilon = 0.05$) and strong radiation ($\varepsilon = 0.80$), and with the three different boundary conditions along BC. The values of all the other parameters are as mentioned at the top of the table. In the weak radiation case there is hardly any effect of the boundary condition on the average convective Nusselt number. However, in the strong radiation case, there is a strong influence of the boundary condition on the average convective Nusselt number. It is noted that the presence of radiation reduces the convective Nusselt number, an observation that is in broad agreement with the findings of earlier studies. Total Nusselt number is not affected significantly by the type of boundary condition in the weak radiation case. In the strong radiation case there is a significant effect of the boundary condition on the total Nusselt number. This is entirely due to the strong influence of the boundary condition on the radiation Nusselt number.

4.3. Effect of the height of computational domain

The computational domain considered in this case is (1) + (2) + (3). Boundary condition (III) is chosen along BE. Since the total number of grids is held fixed, the number

of grids in the domain (1) + (2) changes to 31×41 with 31×11 in the extended domain (3).

The strong radiation case with $\varepsilon = 0.85$ is considered, with all other parameters held fixed at the values that were used in the cases presented in Fig. 5(a)–(c). The flow and temperature fields for three different cases of height of computational domain equal to H—computational domain (1) + (2), $3H/2$ and $2H$—computational domain (1) + (2) + (3), indicate that there is hardly any effect of the extension of the boundary beyond AC. In view of the above the computational domain is limited to (1) + (2) with boundary condition (III) applied along BC, in the rest of the present study.

5. Validation

The validations given below correspond to limiting forms of the right vented top open cavity when (a) the vent wall is either as tall as the left wall or (b) when it is totally absent.

5.1. Validation for convection and radiation in an open-top cavity

When the right side vent wall height is the same as the height of the left hot wall the geometry considered in the present study corresponds to a top open cavity that has been considered earlier [11,15]. Present results for typical values of various parameters are compared with the experimental results of [15]. For example, at a median value of Rayleigh number of 6.8×10^5, $N_{rc} = 39.14$ and low emissivity walls with $\varepsilon = 0.05$, the present calculation yields a value of 15.42 for the mean convection Nusselt number that compares very favorably with the experimental value of 15.11. However the correlation proposed in [11] yields a significantly lower value of 13.64 for the same set of parameters.

5.2. Comparison with experimental and numerical data in a L-shaped geometry

When the right wall is removed altogether, the geometry is the same as the L-corner studied earlier by various authors. For example, Balaji and Venkateshan [14] made use of a computational domain that extended the bottom boundary to a width equal to that of the bottom adiabatic wall. The boundary was not extended in the vertical direction. They proposed a correlation based on their calculations in the *range* 5×10^5–2×10^6. The present computations are based on truncating the computational domain to the width of the bottom adiabatic wall and the imposition of the mixed boundary condition (III) along the right open boundary. The isotherm patterns obtained here compare very closely with those presented in [14]. Also the heat transfer data shows a very good agreement as shown in Fig. 6. The figure also shows the results of Angirasa and Mahajan [10] and Rodighiero and de Socio [4], The trend lines

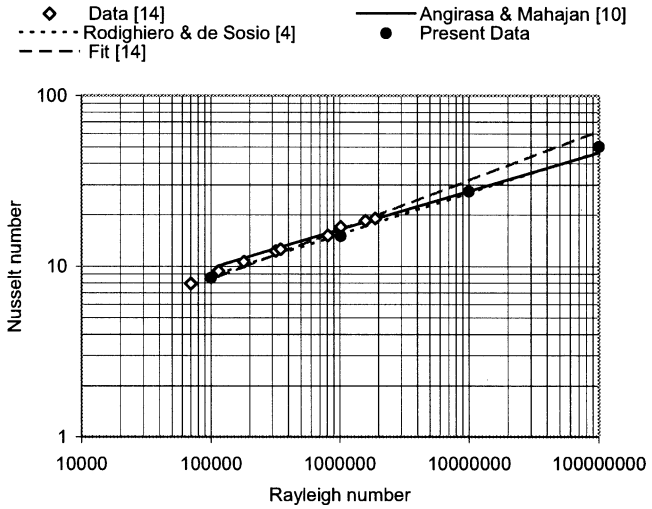

Fig. 6. Nusselt number comparisons for the L-corner.

due to these authors as reported in Balaji and Venkateshan [14] agree very closely with the present data shown for four Rayleigh numbers, viz., 10^5, 10^6, 10^7 and 10^8. The fit to the data of Balaji when extrapolated for higher Rayleigh numbers tends to over estimate the results. These comparisons vindicate the use of truncated computational domain and the use of the mixed boundary condition along the right open boundary.

5.3. Validation with experimental results of Ramesh and Merzkirch [1]

Further validation is possible with the experimental results of Ramesh and Merzkirch [1]. They have presented results for a narrow range of Rayleigh numbers and for $A = 2$, $W = 0.25$, 0.5 and $\varepsilon = 0.05$, 0.85. The paper also presents very limited data on heat transfer from the left hot wall. A typical case considered in [1] corresponds to the following parameter set: $H = 0.07$ m, $d = 0.035$ m, $T_\infty = 293$ K, $\Delta T = 43\,^\circ$C, $\varepsilon = 0.05$ and 0.85. The total Nusselt numbers corresponding to the low emissivity case are 16.1 (present study) and 17 [1] while the corresponding numbers for high emissivity case are 26.4 and 28.7, respectively. From this it may be concluded that the agreement between the present computations with the experimental values is very good. In problems that involve interaction between convection and radiation it is also important to look at the relative share of convection and radiation heat transfer in the total heat transfer. Fig. 7 shows the variation of the percentage of heat transferred by natural convection and radiation with Rayleigh number for the low emissivity case and for two W values. There is an excellent agreement with the present calculations and the experimental results. The results also indicate that the vent wall height represented by W does not have any significant effect on the apportioning of the heat transferred form the left wall between convection and radiation. From Fig. 8 it is apparent that there is an excellent match between the present results and those in

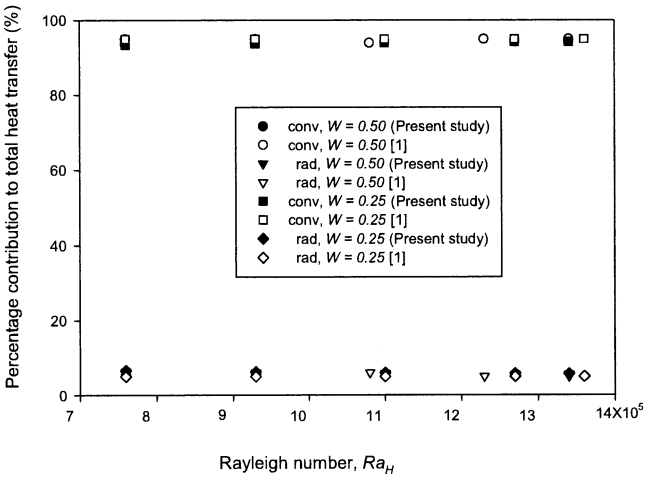

Fig. 7. Effect of side vent on the percentage of heat transferred by convection and radiation from the left wall for $A = 2$, $\varepsilon = 0.05$.

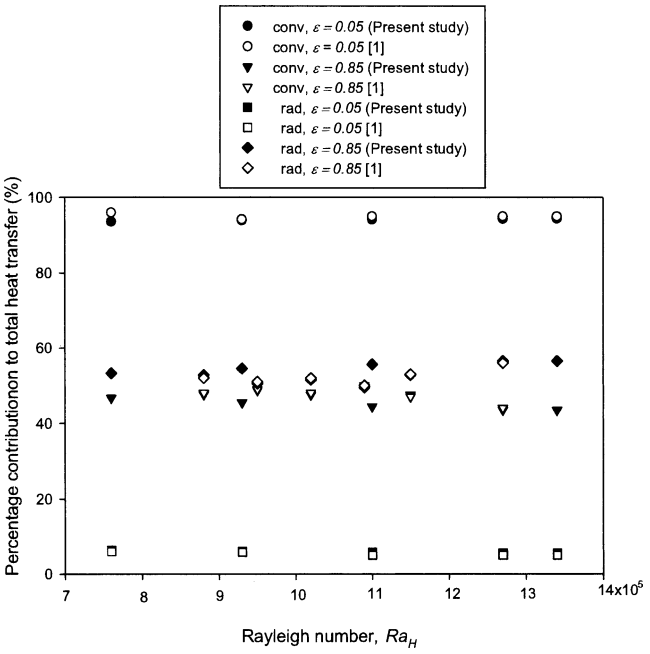

Fig. 8. Effect of surface emissivity on the percentage of heat transferred by convection and radiation for $A = 2$, $W = 0.5$.

Ramesh and Merzkirch [1] for the high emissivity case also. The ordinate shows the percentage of heat transferred by natural convection and surface radiation. The percentages have been computed with respect to the total heat transferred from the left wall of the cavity.

6. Typical results for side-vented top open cavity

Having validated the present code with previous studies available in the literature, a detailed parametric study has been undertaken. Typical results from this study are presented here for a side-vented top open cavity with highly

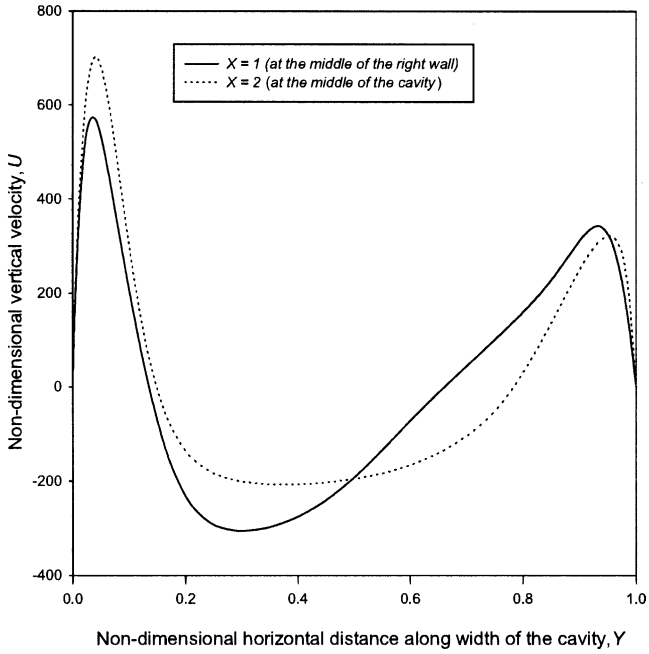

Fig. 9. Vertical velocity profiles across the cavity across two sections for $Ra_H = 1.075 \times 10^6$, $A = 4$, $W = 0.5$, $\varepsilon = 0.85$, $T_R = 0.844$ and $N_{rc} = 10.774$.

emitting walls. The parameter set is taken as $Ra_H = 1.075 \times 10^6$, $\varepsilon = 0.85$, $A = 4$, $W = 0.5$, $T_R = 0.844$, $N_{rc} = 10.774$.

6.1. Streamline and isotherm patterns for side-vented cavities

Fig. 5(c) has already shown the streamline and isotherm contours for the above set of parameters (but with $\varepsilon = 0.8$). Streamline pattern indicates that the fluid enters from the top as well from the port region (BC) of the extended domain above the right wall. Some of the fluid entering from the right comes down into the cavity and rises up after picking up heat. It is seen that two flow loops are formed in the cavity due to thermal boundary layer formation on *all* the cavity walls. Streamlines cut the dashed line (AC in Fig. 1) at different angles showing the effect of the correct boundary condition. Isotherm contours show the development of thermal boundary layers along the left isothermal wall, bottom and right adiabatic walls. The development of thermal boundary layers along the highly emissive adiabatic walls of the cavity provides proof for the existence of radiative interactions among the walls that form the cavity.

6.2. Variation of vertical velocity (U)

Fig. 9 shows the variation of dimensionless vertical velocity across two different sections along the height of the cavity. The velocity profiles show that boundary layers form adjacent to the left and right walls located at $X = 1, 2$. Two peaks are observed, larger one near the heated left wall

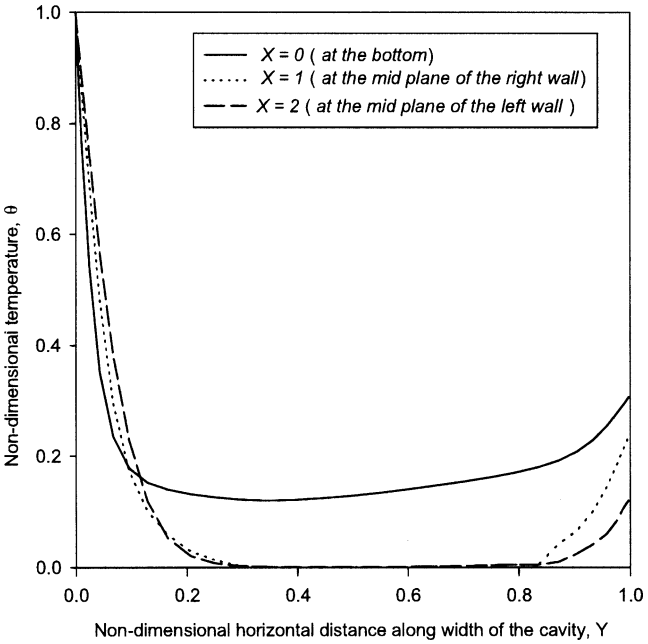

Fig. 10. Temperature profiles across the cavity at different sections for $Ra_H = 1.075 \times 10^6$, $A = 4$, $W = 0.5$, $\varepsilon = 0.85$, $T_R = 0.844$, $N_{rc} = 10.774$.

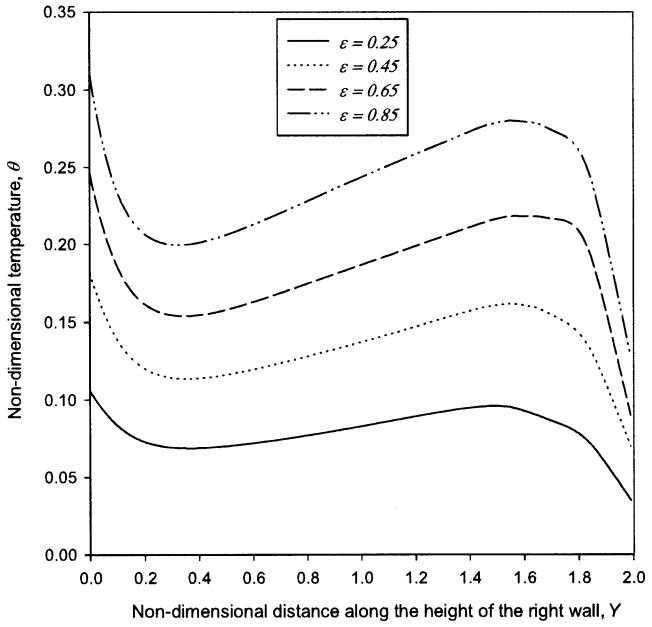

Fig. 11. Local temperature distributions along the height of the right wall $Ra_H = 1.057 \times 10^6$, $A = 4$, $W = 0.5$, $\varepsilon = 0.85$, $T_R = 0.844$, $N_{rc} = 10.774$.

and a second smaller one close to the right adiabatic wall. Radiation heat transfer from the left wall heats both the right and the bottom walls, and, under equilibrium, these two walls lose heat convectively to air. Thus there are two plumes leaving the cavity. However, the streamline pattern indicates that some of the fluid moving parallel to the right wall leaves from the side just above the right wall after interacting with the flow into the cavity across the opening.

6.3. Temperature distribution across the cavity

Fig. 10 shows the temperature distributions across three different sections of the cavity at $X = 0, 1, 2$. It is seen that the bottom wall ($X = 0$) is substantially heated because of radiation whereas the air temperature across a substantial portion of the cavity is at the ambient temperature, except in the boundary layer regions near the left hot wall and the radiantly heated adiabatic right wall.

6.4. Temperature distribution along the right wall

The temperature distribution along the right wall, for the same set of parameters as considered above, is shown in Fig. 11. This figure indicates a rise in temperature of the right adiabatic wall above the ambient temperature. The dimensionless temperature first decreases and then increases and drops at the top of the wall. The temperature distribution is achieved because of a balance between radiation the wall receives and the convective heat it loses. The temperature distribution along the wall mirrors the variation of radiant heating along its length. In general the temperature of the right wall increases with emissivity.

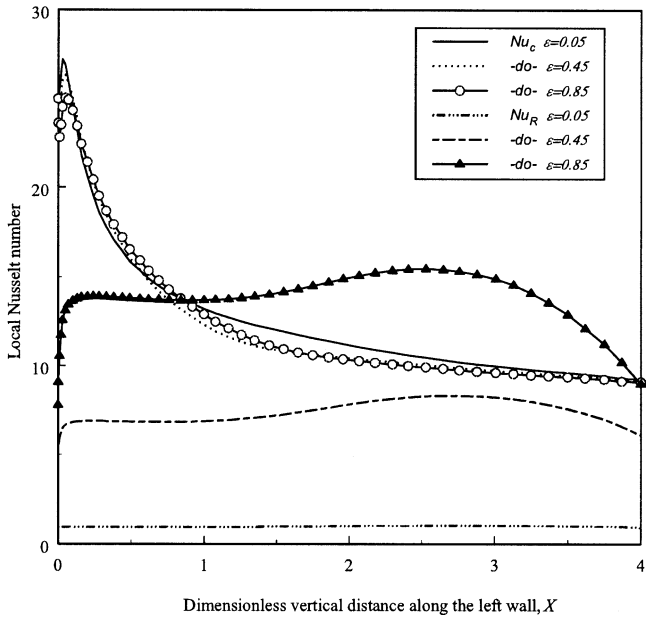

Fig. 12. Local convective and radiative Nusselt number distributions along the left wall for $Ra_H = 1.075 \times 10^6$, $A = 4$, $W = 0.5$, $\varepsilon = 0.85$, $T_R = 0.844$, $N_{rc} = 10.774$.

6.5. Local convective and radiative Nusselt number variation along the left wall ($A = 4$, $W = 0.50$, $T_R = 0.844$, $N_{rc} = 10.77$, $Ra_H = 1.075 \times 10^6$)

Fig. 12 shows the local convective and radiative Nusselt number distribution along the left wall for the above set of parameters. It can be seen that convective Nusselt number reaches a maximum very close to the bottom and then decreases continuously as one proceeds up along the surface.

As the surface emissivity increases, the convective Nusselt number decreases marginally. The higher value of surface emissivity causes a reduction of convective heat transfer from the left wall, but at the same time, increases radiative heat transfer from the left wall, because of intense surface radiation interchange among the walls of the cavity. In a cavity with highly emissive walls, the walls get heated due to surface radiation. Thus the air close to all the walls of the cavity get heated due to convection. In other words, convective heating of the air takes place due to radiative heating of the walls. Figure shows that the radiative Nusselt number increases as surface emissivity increases. However, the mean convective Nusselt number changes marginally with emissivity.

7. Correlations

The ranges of parameters for which calculations have been done are shown in Table 1. All the walls were assumed to have the same emissivity. Based on a large set of numerical data (some 50 data sets in all), correlation for average convection Nusselt number has been derived as

$$\overline{Nu}_c = 0.359 Gr_H^{0.275} \left[\frac{N_{\rm rc}}{N_{\rm rc}+1}\right]^{0.14} \times (1+\varepsilon)^{-0.035} A^{-0.26} (1+W)^{-0.057} \quad (17)$$

As Grashof number directly affects convection heat transfer power law form is used for $Gr_H \cdot N_{\rm rc}$ is a superfluous parameter if only one fluid is considered. But if the temperature level changes, while the temperature difference between the left wall and ambient remains the same, then $\overline{Nu}_c$ will be affected because of radiative effects. The exponent of aspect ratio (A) is negative, which signifies $\overline{Nu}_c$ decreases with increase in aspect ratio.

In evolving the above correlation, $(1+\varepsilon)$ has been used as the most appropriate form for ε, because, even when $\varepsilon = 0$, $\overline{Nu}_c$ would be non-zero, as it still contains natural convection component and the term has a moderate negative exponent, which means that convection decreases with ε. In the above correlation, $(1+W)$ has been used as the form for W because, even when $W = 0$, $\overline{Nu}_c$ would be non-zero. The exponent of $(1+W)$ is very small. A very high correlation coefficient of 0.998 and a standard error of 0.129 indicate the goodness of the fit.

Average radiation Nusselt number ($\overline{Nu}_R$), is correlated as

$$\overline{Nu}_R = 0.261 Gr_H^{0.179} \left[1 - T_R^4\right]^{0.4} N_{\rm rc}^{0.48} \varepsilon^{0.94} A^{0.59} \times (1+W)^{-0.38} \quad (18)$$

As ε increases $\overline{Nu}_R$ increases and hence the power law form is used for ε. With reference to T_h^4, it appears in the $N_{\rm rc}$ term. Heat flux is proportional to $(T_h^4 - T_\infty^4)$. This can be also written in the form as $T_h^4(1 - T_R^4)$ where $T_R = (T_\infty/T_h)$. Hence, the temperature ratio is correlated in the form given above. Aspect ratio (A) follows power law and its exponent is large and therefore $\overline{Nu}_R$ is greatly influenced by A. The form of W and its influence is similar to that encountered in the correlation for $\overline{Nu}_c$. The influence of convection is brought out by the term involving the Grashof number. The goodness of the fit is indicated by a very high value of correlation coefficient of 0.998 and a standard error of 0.205. In order to conserve space parity plots are not presented here. Such plots show that the numerical data is distributed around the parity line without any bias. Also the uncertainties in using the correlating equations is no more than $\pm 1.5\%$. Range of parameters for which the correlations are valid are as given in Table 1.

8. Conclusions

From the present study, the following conclusions are made:

(1) Mixed boundary condition is found to be the proper one for the opening above the right wall.
(2) Emissivity of the walls affects the heat transfer to a larger extent than the right side wall height and the cavity aspect ratio.
(3) For low emissivities radiation part is only about 5% of the total heat loss from the left heated wall while it is comparable to the convective part for high emissivities.
(4) Thermal and velocity boundary layers develop along *all* the walls of the cavity. This is a consequence of surface radiation and its interaction with convection.
(5) Useful correlations are presented for heat transfer from the left wall, based on large number of calculations encompassing a useful range for various parameters that affect the problem.

References

[1] N. Ramesh, W. Merzkirch, Combined convective and radaitive heat transfer in side-vented open cavities, Internat. J. Heat Fluid Flow 22 (2001) 180–187.
[2] J.H. Van Leeuwan, C. Looma, J. Schenk, Experimental study of velocity and temperature distributions for free convection in a corner, Internat. J. Heat Mass Transfer 14 (1971) 561–564.
[3] P. Le Quere, J.A.C. Kumphrey, F. Sherman, Numerical calculation of thermally driven two-dimensional unsteady laminar flow in cavities of rectangular cross section, Numer. Heat Transfer 4 (1981) 249–283.
[4] C. Rodighiero, L.M. de Socio, Some aspects of natural convection in a corner, ASME J. Heat Transfer 105 (1983) 212–214.
[5] Y.L. Chan, C.L. Tien, A numerical study of two-dimensional laminar convection in shallow open cavities, Internat. J. Heat Mass Transfer 28 (1985) 601–612.
[6] A.H. Abib, Y. Jaluria, Numerical simulation of the buoyancy-induced flow in a partially open enclosure, Numer. Heat Transfer 14 (1988) 235–254.
[7] M. Behnia, G. de Vahl Davis, Natural convection cooling of an electronic component in a slot, in: Proceedings of the 9th International Heat Transfer Conference, vol. 2, Jerusalem, 1990, pp. 343–348.

[8] F. Penot, A. Noame, P. Le Quere, Investigation of the route to turbulence in a vertical differentially heated open cavity, in: Proceedings of the 9th International Heat Transfer Conference, vol. 2, Jerusalem, 1990, pp. 417–422.
[9] J.L. Lage, J.S. Lim, A. Bejan, Natural convection with radiation in a cavity with open top end, ASME J. Heat Transfer 114 (1992) 479–486.
[10] D. Angirasa, R.L. Mahajan, Natural convection from L-shaped corners with adiabatic and cold isothermal walls, ASME J. Heat Transfer 115 (1993) 149–157.
[11] C. Balaji, S.P. Venkateshan, Interaction of radiation with free convection in an open cavity, Internat. J. Heat Fluid Flow 15 (4) (1994) 317–324.
[12] A.A. Mahamad, Natural convection in open cavities and slots, Numer. Heat Transfer Part A 27 (1995) 705–716.
[13] A.A. Dehgan, M. Behnia, Combined natural convection conduction and radiation heat transfer in a discretely heated open cavity, ASME J. Heat Transfer 118 (1996) 56–64.
[14] C. Balaji, S.P. Venkateshan, Free convection with surface radiation and conduction in an L-corner, ASME J. Heat Transfer 118 (1996) 222–225.
[15] N. Ramesh, C. Balaji, S.P. Venkateshan, An experimental study of natural convection and surface radiation in an open cavity, Heat Technology Calore Technol. 19 (2001) 89–94.
[16] O. Polat, E. Bilgen, Laminar natural convection in inclined shallow cavities, Internat. J. Thermal Sci. 41 (2002) 360–368.
[17] C. Gururajarao, C. Balaji, S.P. Venkateshan, Numerical study of laminar mixed convection from a vertical plate, Internat. J. Transport Phenomena 2 (2000) 143–157.
[18] H.C. Hottel, A.S. Sarofim, Radiative Heat Transfer, McGraw-Hill, New York, 1967.
[19] A.D. Gosman, Pun W.M. Runchal, A.K. Spalding, D.B. Wolfshtein, Heat and Mass Transfer in Recirculating Flows, Academic Press, London, 1969.